Langmuir Article

pubs.acs.org/Langmuir

Thermal Stability of Mono-, Bis-, and Tris-Chelating Alkanethiol Films Assembled on Gold Nanoparticles and Evaporated "Flat" Gold

La-ongnuan Srisombat, Shishan Zhang, and T. Randall Lee*

Departments of Chemistry and Chemical Engineering, University of Houston, 4800 Calhoun Road, Houston, Texas 77204-5003

Received June 10, 2009. Revised Manuscript Received August 21, 2009

The thermal stability of SAMs generated from the adsorption of *n*-octadecanethiol (***n*-C18**), 2-hexadecylpropane-1,3-dithiol (**C18C2**), 2-hexadecyl-2-methylpropane-1,3-dithiol (**C18C**3), and 1,1,1-tris(mercaptomethyl)heptadecane (***t*-C18**) on colloidal gold and evaporated "flat" gold was investigated. The optical extinction of the monolayer-protected nanoparticles (MPCs) was monitored as a function of thermal stress by using ultraviolet−visible (UV−vis) spectroscopy, which revealed that the evolution of the surface plasmon resonance varied with the nature of the adsorbate. Specifically, MPCs functionalized with monodentate ***n*-C18** showed the fastest red shift of the surface plasmon resonance while those functionalized with tridentate ***t*-C18** showed the slowest red shift, with those derived from the bidentates **C18C2** and **C18C3** falling in between, suggesting a correlation between film stability and the degree of chelation. In separate studies, X-ray photoelectron spectroscopy (XPS) was used to evaluate the desorption of the monolayers on both colloidal gold and flat gold as a function of thermal stress. In these studies, SAMs generated from monodentate ***n*-C18** showed the fastest desorption while SAMs generated from tridentate ***t*-C18** showed the slowest desorption, with those derived from the bidentates **C18C2** and **C18C3** falling in between, again suggesting a correlation between film stability and the degree of chelation. As a whole, the following trend in thermal stability was observed: ***t*-C18** > **C18C2** ≈ **C18C3** > ***n*-C18**.

Introduction

Due in part to their facile preparation and characterization, self-assembled monolayers (SAMs) generated by the adsorption of alkanethiols on gold have been the subject of extensive research.[1−3] Apart from a unique opportunity to stabilize metal nanoparticles by isolating them from their environment, where the possibility of particle aggregation can be significantly reduced,[4] SAMs are also potentially useful in a number of technologies that range from corrosion prevention[5,6] to chemical sensing[7] and microelectronic device fabrication.[8,9] In such applications, the thermal and/or long-term stability of SAMs is a critical factor. Studies have shown that SAMs on gold derived from *n*-alkanethiols offer only finite stability, which restricts their usefulness to applications where robust coverage is not required. Specifically, SAMs on gold exhibit moderate stability at room temperature[10,11] but decompose rapidly at elevated temperatures.[12]

Several approaches have been explored to enhance the stability of SAMs on gold, including the use of (1) absorbates that employ multiple sulfur−gold interactions,[13−20] (2) underpotential metal deposition,[21,22] and (3) cross-linking moieties within the alkyl chains (e.g., lateral polymerization, hydrogen bonding, and π stacking).[14,15,23−27] Adsorbates that possess the ability to bind to the surface of gold via multiple sites can enhance the stability of SAMs via the entropy-driven chelate effect;[28,29] moreover, multidentate chelating adsorbates can be designed to resist the formation of intramolecular disulfides upon desorption from the surface.[14−20,30−32] Along these lines, our group has been exploring the formation and characterization of SAMs on evaporated "flat" gold derived from the adsorption of various multidentate alkanethiols,[14−20] where selected prototypical structures are

*To whom correspondence should be addressed. Email: trlee@uh.edu.

(1) Daniel, M.-C.; Astruc, D. *Chem. Rev*. **2004**, *104*, 293.
(2) Love, J. C.; Estroff, L. A.; Kriebel, J. K.; Nuzzo, R. G.; Whitesides, G. M. *Chem. Rev*. **2005**, *105*, 1103.
(3) Ulman, A. *An Introduction to Ultrathin Organic Films: from Langmuir-Blodgett to Self-Assembly*; Academic: Boston, MA, 1991.
(4) Balasubramanian, R.; Kim, B.; Tripp, S. L.; Wang, X.; Lieberman, M.; Wei, A. *Langmuir* **2002**, *18*, 3676.
(5) Zamborini, F. P.; Campbell, J. K.; Crooks, R. M. *Langmuir* **1998**, *14*, 640.
(6) Zamborini, F. P.; Crooks, R. M. *Langmuir* **1998**, *14*, 3279.
(7) Crooks, R. M.; Ricco, A. J. *Acc. Chem. Res*. **1998**, *31*, 219.
(8) Abbott, N. L.; Rolison, D. R.; Whitesides, G. M. *Langmuir* **1994**, *10*, 2672.
(9) Gardner, T. J.; Frisbie, C. D.; Wrighton, M. S. *J. Am. Chem. Soc*. **1995**, *117*, 6927.
(10) Laibinis, P. E.; Whitesides, G. M. *J. Am. Chem. Soc*. **1992**, *114*, 9022.
(11) Kumar, A. K.; Biebuyck, H. A.; Whitesides, G. M. *Langmuir* **1994**, *10*, 1498.
(12) Bain, C. D.; Troughton, E. B.; Tao, Y.-T.; Evall, J.; Whitesides, G. M.; Nuzzo, R. G. *J. Am. Chem. Soc*. **1989**, *111*, 321.
(13) Wooster, T. T.; Gamm, P. R.; Geiger, W. E.; Oliver, A. M.; Black, A. J.; Graig, D. C.; Paddon-Row, M. N. *Langmuir* **1996**, *12*, 6616.
(14) Garg, N.; Lee, T. R. *Langmuir* **1998**, *14*, 3815.
(15) Garg, N.; Carrasquillo-Molina, E.; Lee, T. R. *Langmuir* **2002**, *18*, 2717.
(16) Shon, Y.-S.; Lee, T. R. *J. Phys. Chem. B*. **2000**, *104*, 8182.
(17) Shon, Y.-S.; Lee, T. R. *J. Phys. Chem. B* **2000**, *104*, 8192.
(18) Shon, Y.-S.; Colorado, R., Jr.; Williams, C. T.; Bain, C. D.; Lee, T. R. *Langmuir* **2000**, *16*, 541.
(19) Park, J.-S.; Smith, A. C.; Lee, T. R. *Langmuir* **2004**, *20*, 5829.
(20) Park, J.-S.; Vo, A. N.; Barriet, D.; Shon, Y.-S.; Lee, T. R. *Langmuir* **2005**, *21*, 2902.
(21) Jennings, G. K.; Laibinis, P. E. *Langmuir* **1996**, *12*, 6173.
(22) Jennings, G. K.; Laibinis, P. E. *J. Am. Chem. Soc*. **1997**, *119*, 5208.
(23) Kim, T.; Chan, K. C.; Crooks, R. M. *J. Am. Chem. Soc*. **1997**, *119*, 189.
(24) Clegg, R. S.; Reed, S. M.; Hutchison, J. E. *J. Am. Chem. Soc*. **1998**, *120*, 2486.
(25) Turchanin, A.; El-Desawy, M.; Golzhauser, A. *Appl. Phys. Lett*. **2007**, *90*, 053102.
(26) Sabatani, E.; Cohen-Boulakia, J.; Bruening, M.; Rubinstein, I. *Langmuir* **1993**, *9*, 2974.
(27) Valiokas, R.; Östblom, M.; Svedhem, S.; Svensson, S. C. T.; Liedberg, B. *J. Phys. Chem. B* **2002**, *106*, 10401.
(28) Purcell, K. F.; Kotz, J. C. *Inorganic Chemistry*; W. B. Saunders: Philadelphia, PA, 1977.
(29) Huheey, J. E. *Inorganic Chemistry*; Harper Collins: Singapore, 1983.
(30) Burns, J. A.; Whitesides, G. M. *J. Am. Chem. Soc*. **1990**, *112*, 6296.
(31) Biebuyck, H. A.; Whitesides, G. M. *Langmuir* **1993**, *9*, 1766.
(32) Kolega, R. R.; Schlenoff, J. B. *Langmuir* **1998**, *14*, 5469.

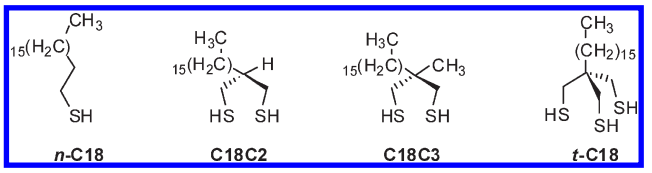

Figure 1. Structures of *n*-octadecanethiol (***n*-C18**), 2-hexadecylpropane-1,3-dithiol (**C18C2**), 2-hexadecyl-2-methylpropane-1,3-dithiol (**C18C3**), and 1,1,1-tris(mercaptomethyl)heptadecane (***t*-C18**).

shown in Figure 1. Recently, the research has been expanded to cover the study of these SAMs adsorbed on gold nanoparticles.[33,34]

When compared to densely packed SAMs generated from normal alkanethiols (***n*-Cn**), SAMs derived from 2-monoalkylpropane-1,3-dithiols (**CnC2**), 2-alkyl-2-methylpropane-1,3-dithiols (**CnC3**), and 1,1,1-tris(mercaptomethyl)alkanes (***t*-Cn**) exhibit a progressively decreasing packing density of the alkyl chains: ***n*-Cn** ≫ **CnC2** > **CnC3** > ***t*-Cn**.[16−20,33,34] Correspondingly, the degree of conformational order (or crystallinity) of these SAMs decreases in the same order. Importantly, a preliminary ellipsometry-based examination of the thermal stability on flat gold indicated that SAMs derived from the tridentate adsorbates (***t*-Cn**) were slightly more thermally stable than those derived from the bidentate adsorbates (**CnC2**, **CnC3**), which were themselves more stable than the SAMs derived from normal alkanethiols (***n*-Cn**).[20] While studies of the thermally induced aggregation of large gold MPCs (i.e., diameters ≥ 20 nm) found a similar trend,[33] independent studies found that adsorbates analogous to ***t*-Cn** can efficiently block ligand exchange by ***n*-Cn** on small gold MPCs that were ∼3−5 nm in diameter.[35] Interestingly, an examination of the chemical stability of small MPCs, as evaluated by cyanide-induced decomposition, found a somewhat different trend: **CnC3** ≫ **CnC2** > ***t*-Cn** ≫ ***n*-Cn**.[34]

Given this background, the aim of the present work is to provide a definitive evaluation of the thermal stability of SAMs on both gold nanoparticles and flat gold as a function of the degree of chelation of the adsorbate. In particular, given the inconsistencies noted above, we wished to examine the thermal stability on gold having essentially no macroscopic curvature (i.e., evaporated gold on silicon wafers) and gold with the highest curvature possible (i.e., gold nanoparticles ∼2 nm in diameter) to disentangle any effects arising from the morphology of the metal substrate. To this end, we employed the adsorbates shown in Figure 1, octadecanethiol (***n*-C18**), 2-hexadecylpropane-1,3-dithiol (**C18C2**), 2-hexadecyl-2-methylpropane-1,3-dithiol (**C18C3**), and 1,1,1-tris(mercaptomethyl)heptadecane (***t*-C18**), to vary the degree of chelation in a systematic fashion. We used ultraviolet−visible spectroscopy to monitor the optical properties of the MPCs in solution as a function of both time and temperature. Separately, we used X-ray photoelectron spectroscopy to monitor the atomic composition of the samples.

Experimental Section

Materials. Hydrogen tetrachloroaurate ($HAuCl_4$), toluene, and sodium borohydride ($NaBH_4$) were purchased from EM Sciences. Water was purified to a resistance of 18 MΩ by an Academic Milli-Q Water System (Millipore Corporation) and filtered through a 0.22 μm membrane filter before use. Absolute ethanol (Aaper Alcohol), carbon tetrachloride (CCl_4; Acros), tetraoctylammonium bromide (Aldrich), and *n*-octadecanethiol (***n*-C18**; TCI America) were purchased from the indicated suppliers and used as received. The adsorbates 2-hexadecyl-2-methylpropane-1,3-dithiol (**C18C2**), 2-hexadecyl-2-methylpropane-1,3-dithiol (**C18C3**), and 1,1,1-tris(mercaptomethyl)trihexadecane (***t*-C18**) were prepared as described previously.[16,18,19] Gold was purchased from Americana Precious Metals, and polished single-crystal silicon(100) wafers were purchased from Silicon Sense, Inc.

Preparation of SAMs on Flat Gold. The experimental procedures used to generate and characterize the SAMs have been described in detail in our previous reports.[16−20] Briefly, the gold substrates were prepared by the thermal evaporation of 1000 Å of gold onto silicon wafers at a rate of 1 Å/s. Before the vapor deposition of gold, the silicon wafers were precoated with 100 Å of chromium to promote the adhesion of gold. A quartz oscillator was used to monitor the evaporation rates and deposition thicknesses. The gold-coated silicon wafer slides (ca. 1×4 cm^2) were washed with ethanol and dried with ultrapure nitrogen gas before use. The vials used to prepare the SAMs were cleaned with "piranha" solution (3:1, H_2SO_4/H_2O_2) for 1 h, washed with deionized water and ethanol, and dried in an oven at ∼100 °C prior to use. (*Caution: Piranha solution is extremely hazardous; it should be handled with great care and never stored in a sealed container*.) A 1 mM solution of ***n*-C18**, **C18C2**, and **C18C3** was prepared using ethanol as a solvent, while a 1 mM solution of ***t*-C18** was prepared in THF. The gold-coated slides were immersed in the solution and allowed to equilibrate for 48 h. The slides were then rinsed thoroughly with toluene and ethanol and dried with a stream of ultrapure nitrogen before characterization.

Preparation of MPCs Coated with *n*-C18. All glassware was cleaned in aqua regia (3:1, HCl/HNO_3) for at least 1 h (*Caution*: *Aqua regia is extremely hazardous*; *it should be handled with great care*.), thoroughly rinsed with deionized water and acetone, and then dried in an oven at ∼100 °C prior to use. The monolayer-protected gold nanoparticles were synthesized using a modified Brust−Schiffrin procedure.[36,37] A 2.00 mL aliquot of a 1.0% aqueous solution of $HAuCl_4$ (0.051 mmol) was transferred to a 25 mL round-bottomed flask. A 1.70 mL aliquot of a 7.5×10^{-2} M solution of tetraoctylammonium bromide ($(C_8H_{17})_4NBr$, 0.13 mmol) in toluene was added to the vigorously stirred solution. Stirring was maintained for at least 15 min to ensure complete phase transfer of the gold salt, which was confirmed visually by observing the disappearance of a pale yellow color from the aqueous phase and the appearance of the reddish orange color to the organic phase. A 0.89 mL aliquot of a 1.9×10^{-2} M solution of *n*-octadecanethiol (0.017 mmol) in toluene was added dropwise to the organic phase. To the vigorously stirred mixture, a 5.72 mL aliquot of a 0.11 M aqueous solution of sodium borohydride (0.63 mmol) was then added dropwise over 15 min. The color of the organic phase immediately changed from reddish-orange to dark violet. The resulting solution was stirred overnight at room temperature. The aqueous phase was removed using a disposable pipet, and the organic phase was concentrated to ∼1 mL by rotary evaporation. The remaining mixture was diluted with 30 mL of absolute ethanol and stored at −50 °C for at least 4 days to induce the functionalized gold nanoparticles to precipitate from the mixture.

Preparation of MPCs Coated with C18C2, C18C3, and *t*-C18. The procedure detailed above was employed with substitution of a 1.05 mL aliquot of a 8.1×10^{-3} M of **C18C2** (0.0085 mmol), a 1.05 mL aliquot of a 8.1×10^{-3} M solution of **C18C3** (0.0085 mmol), or a 0.73 mL aliquot of a 7.7×10^{-3} M solution of ***t*-C18** (0.0056 mmol). The molar ratio of sulfur to gold was maintained at 1:3 for each reaction to produce functionalized nanoparticles having similar sizes (i.e., ∼2 nm). Before performing

(33) Zhang, S.; Leem, G.; Srisombat, L.; Lee, T. R. *J. Am. Chem. Soc.* **2008**, *130*, 113.
(34) Srisombat, L.; Park, J.-S.; Zhang, S.; Lee, T. R. *Langmuir* **2008**, *24*, 7750.
(35) Wojczykowski, K.; Meissner, D.; Jutzi, P.; Ennen, I.; Hütten, A.; Fricke, M.; Volkmer, D. *Chem. Commun.* **2006**, 3693.
(36) Brust, M.; Walker, M.; Bethell, D.; Schiffrin, D. J.; Whyman, R. *J. Chem. Soc., Chem. Commun.* **1994**, 801.
(37) Brust, M.; Fink, J.; Bethell, D.; Schiffrin, D. J.; Kiely, C. *J. Chem. Soc., Chem. Commun.* **1995**, 1655.

the thermal stability studies, all of the MPCs were fully characterized using (UV−vis) spectroscopy, transmission electron microscopy (TEM), X-ray photoelectron spectroscopy (XPS), and Fourier-transform infrared (FT-IR) spectroscopy.[34]

Solution Thermolysis and Displacement of MPCs. The optical properties of the MPCs as a function of thermal treatment in decalin at 80, 100, and 120 °C were monitored by UV−vis spectroscopy over the range 300 to 1100 nm using a Cary 50 scan UV−vis optical spectrometer (Varian) with Cary Win UV software. UV−vis spectra were recorded at room temperature by placing aliquots of the samples in a quartz cell having a 1 cm optical path length. Separate studies of monolayer displacement were performed in decalin with prolonged heating at 120 °C. For each solution of the four MPCs, all four thiols (***n*-C18**, **C18C2**, **C18C3**, ***t*-C18**) were used as displacing agents. In these studies, the thiol-displacing agent was added to the MPC solution so that the final concentration of thiol-displacing agent was maintained at 1 mM. UV−vis spectroscopy was used to monitor the optical absorbance of the latter solutions as a function of time.

Analysis by XPS. XPS spectra were collected using a PHI 5700 X-ray photoelectron spectrometer equipped with PHI 04091 neutralizer and a monochromatic Al Kα X-ray source ($h\nu$ = 1486.7 eV) incident at 90° relative to the axis of a hemispherical energy analyzer. The spectrometer was operated at high resolution with a pass energy of 23.5 eV, a photoelectron takeoff angle of 45° from the surface, and an analyzer spot diameter of 1.1 mm. The base pressure in the chamber during the measurements was 1×10^{-9} Torr. SAMs on colloidal gold were dispersed in CCl_4 and spotted onto a silicon wafer. After the solvent evaporated to dryness at room temperature, the samples were transferred to the measurement chamber. The SAMs on flat gold were cut into squares (1×1 cm^2) and characterized using contact angle goniometry and ellipsometry to ensure the quality of the film was consistent with previous reports.[20] The samples were then mounted on a sample holder having a small resistive button heater to allow heating under vacuum between measurements. The heater was equipped with a thermocouple to allow precise control of the temperature. The samples were brought to a desired temperature and were maintained at that temperature for 5 min. After cooling to room temperature, XPS data were collected. We referenced the binding energies by setting the $Au_{4f7/2}$ binding energy to 84.0 eV. All sulfur peaks were fit with respect to spin−orbit splitting. Standard curve-fitting software (Multipak V5.0A; Physical Electronics, Inc.) using Shirley background subtraction and Gaussian−Lorentzian profiles was used to determine the peak intensities.

Results and Discussion

Thermolysis of MPCs. UV−vis spectroscopy is a common tool for monitoring the surface plasmon resonance bands of nanoparticles.[38−40] Importantly, for gold nanoparticles, the optical properties of the surface plasmon band depend strongly on their size.[41] For the nanoparticles in this study (~2 nm in diameter), the plasmon band is centered at 515 nm (data not shown), which is in agreement with that previously reported for gold particles having similar sizes and prepared using the two-phase method.[42] For all the adsorbates examined in this study, prolonged heating of the solutions at 80 and 100 °C for two days led to no substantial changes in the shape or position of the plasmon band and no change in the color of the solution (data not shown). These results are also in agreement with those previously reported[39] and illustrate the robust nature of MPCs at these temperatures. Upon heating to 120 °C, however, the MPCs undergo structural changes, and the plasmon bands shift to longer wavelengths. Figure 2 shows the shifting of the plasmon bands as a function of time during the heating process. This shift is likely associated with agglomeration of the particles as proposed by Maye and co-workers.[39] The color of the solutions evolved from brown to red to purple, coincident with the production of less-soluble/insoluble products. Research has shown that changes in intensity and wavelength of the surface plasmon bands are reliable indicators of changes in particle size, interparticle distance, and/or dielectric properties of the solution.[43] For the MPCs heated to 120 °C in our studies, the evolution of the plasmon band as a function of time revealed an initial increase in absorbance and position followed by a gradual decrease in absorbance (data not shown). We observed this trend for all of the absorbates examined. Others have proposed that this behavior arises from a three-step nanoparticle growth process involving (1) ligand desorption, (2) metal core coalescence, and (3) ligand re-encapsulation.[39,40] It is also well documented that the plasmon band undergoes red shifting and band broadening during particle agglomeration.[43,44] In our analysis, we monitor the red shift and use it to indicate the stability of the MPCs under thermal stress.

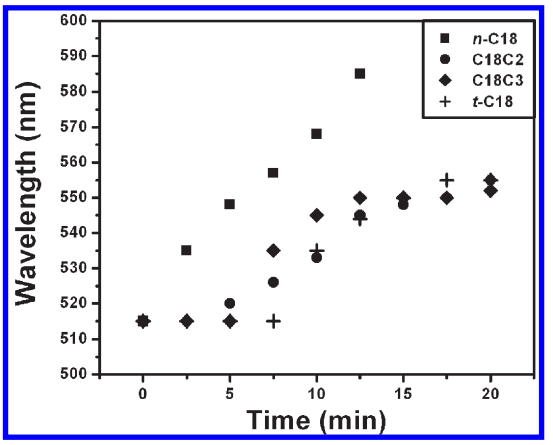

Figure 2. Evolution of the absorbance maximum upon heating the indicated MPCs in decalin at 120 °C.

Figure 2 shows that the MPCs functionalized with ***n*-C18** exhibit the most rapid shift of the surface plasmon resonance upon heating at 120 °C. In contrast, those functionalized with **C18C2**, **C18C3**, and ***t*-C18** exhibit slower shifts, suggesting an enhanced thermal stability afforded by the latter adsorbates. Unfortunately, the data are insufficiently resolved to distinguish any differences in stability between the multidentate adsorbates, which led us to explore displacement studies as a means of determining their relative thermal stabilities.[17]

Displacement Studies. To examine the displacement of one ligand for another, we added a selected displacing agent to a selected MPC in decalin and then heated the mixture to 120 °C. The evolution of the surface plasmon bands was recorded by UV−vis spectroscopy. Figure 3a shows that the shift in the plasmon band of the MPCs generated from ***n*-C18** and exposed to 1 mM displacing agents occurs most rapidly when ***n*-C18** is added and gives the following overall trend in stability:

(38) Porter, L. A., Jr.; Ji, D.; Westcott, S. L.; Graupe, M.; Czernuszewicz, R. S.; Halas, N. J.; Lee, T. R. *Langmuir* **1998**, *14*, 7378.
(39) Maye, M. M.; Zheng, W.; Leibowitz, F. L.; Ly, N. K.; Zhong, C. J. *Langmuir* **2000**, *16*, 490.
(40) Maye, M. M.; Zhong, C. J. *J. Mater. Chem.* **2000**, *10*, 1895.
(41) Alvarez, M. M.; Khoury, J. T.; Schaaff, T. G.; Shafigullin, M. N.; Vezmar, I.; Whetten, R. L. *J. Phys. Chem. B* **1997**, *101*, 3706.
(42) Hostetler, M. J.; Wingate, J. E.; Zhong, C.-J.; Harris, J. E.; Vachet, R. W.; Clark, M. R.; Londono, J. D.; Green, S. J.; Stokes, J. J.; Wignall, G. D.; Glish, G. L.; Porter, M. D.; Evans, N. D.; Murray, R. W. *Langmuir* **1998**, *14*, 17.
(43) Luo, J.; Maye, M. M.; Han, L.; Kariuki, N. N.; Jones, V. W.; Lin, Y.; Engelhard, M. H.; Zhong, C. J. *Langmuir* **2004**, *20*, 4254.
(44) Weisbecker, C. S.; Meritt, M. V.; Whitesides, G. M. *Langmuir* **1996**, *12*, 3763.

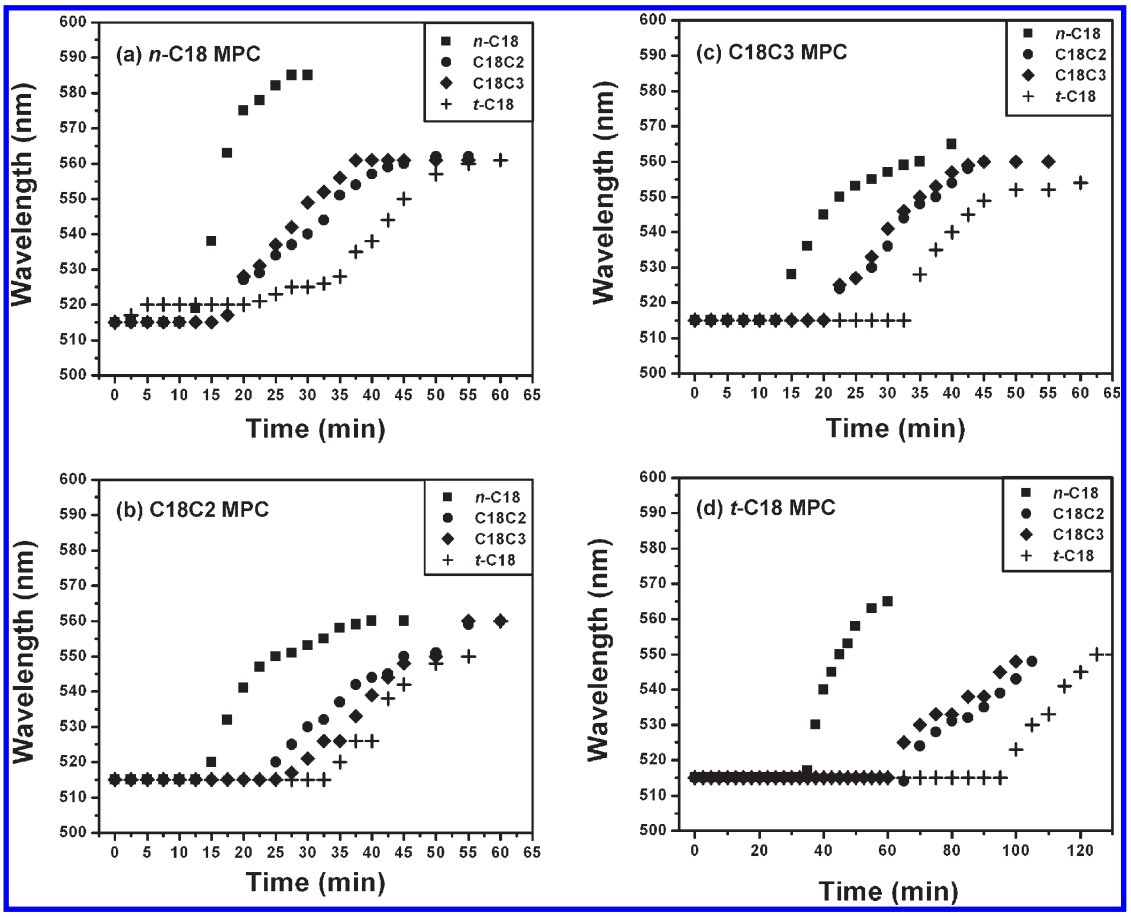

Figure 3. Displacement profiles for MPCs derived from (a) ***n*-C18**, (b) **C18C2**, (c) **C18C3**, and (d) ***t*-C18** upon the addition of the indicated ligands at 120 °C in decalin.

***t*-C18** > **C18C2** ≈ **C18C3** > ***n*-C18**. Interestingly, these results are consistent with the preliminary evaluation of the relative thermal stability of these SAMs on flat gold.[20]

The data in Figure 3b and 3c show that the MPCs generated from **C18C2** and **C18C3** reflect the same trend in thermal stability exhibited by the MPCs generated from ***n*-C18**. Specifically, upon heating the MPCs derived from either **C18C2** or **C18C3**, the red shift of the plasmon band begins after an incubation period of ∼15 min when adding ***n*-C18** as the displacement agent, ∼22 min when adding **C18C2** or **C18C3** as the displacement agent, and ∼30 min when adding ***t*-C18** as the displacement agent. The fact that we are unable to distinguish the relative thermal stability afforded by **C18C2** and **C18C3** contrasts with the relative trend in *chemical* stability observed for these adsorbates, where the methyl group at the branch position of **C18C3**, when compared to the markedly smaller hydrogen atom at the branch position of **C18C2**, appears to sterically inhibit decomposition of the gold core.[34]

The data in Figure 3d provide additional support for the conclusions offered in the preceding paragraphs. Notably, the MPCs generated from ***t*-C18** are substantially slower to undergo agglomeration, with incubation periods of ∼30 min when using ***n*-C18** as a displacing agent, ∼1 h for **C18C2** or **C18C3** as the displacement agent, and ∼1.5 h for ***t*-C18** as the displacement agent. As a whole, the displacement studies indicate the following relative trend in thermal stability afforded by these adsorbates: ***t*-C18** > **C18C2** ≈ **C18C3** > ***n*-C18**, which correlates with the degree of chelation (i.e., tridentate > bidentate > monodentate).

Based on the displacement profiles in Figure 3, we can draw two qualitative conclusions regarding the mechanism of the displacement process. First, desorption of the initial SAM contributes to or is competitive with the rate-determining step; otherwise, the displacement profiles would be invariant toward the nature of the initially adsorbed SAM (i.e., the four displacement profiles in Figure 3a would be the same as those in Figure 3b, which would be the same as those in Figures 3c and 3d). Second, adsorption of the displacing ligand contributes to or is competitive with the rate-determining step; otherwise, the displacement profiles for a given MPC would be invariant toward the nature of the displacing ligand (i.e., all four displacement profiles for a given starting MPC would look the same).

Analysis of SAM-Coated Gold Nanoparticles and Flat Gold by XPS. The use of XPS to evaluate the stability of organosulfur-based SAMs on gold is an established practice.[15,17,45,46] To compare the stability of SAMs generated from the adsorbates in the present study, we monitored the ratio of the sulfur 2p peak areas $(S_{bound}/S_{total})/S_{initial}$, where S_{bound} is the area of sulfur bound to gold at time t, S_{total} is the total area of sulfur at time t, and $S_{initial}$ is the total area of sulfur at $t = 0$ (i.e., before thermolysis). The sulfur 2p peak appears as a 2:1 doublet due to the presence of both S $2p_{3/2}$ and S $2p_{1/2}$.[47] All spectra were therefore fitted using a 2:1 ratio of areas with 1.2 eV separating the peaks. The S $2p_{3/2}$ signal corresponding to bound thiol appears at ∼162 eV,[47,48] and the S $2p_{3/2}$ signal

(45) Buttner, M.; Belser, T.; Oelhafen, P. *J. Phys. Chem. B* **2005**, *109*, 5464.
(46) Ahn, H.; Kim, M.; Sandman, D. J.; Whitten, J. E. *Langmuir* **2003**, *19*, 5303.
(47) Zhou, J.; Beattie, D. A.; Sedev, R.; Ralston, J. *Langmuir* **2007**, *23*, 9170.
(48) Johnson, S. R.; Evans, S. D.; Mahon, S. W.; Ulman, A. *Langmuir* **1997**, *13*, 51.

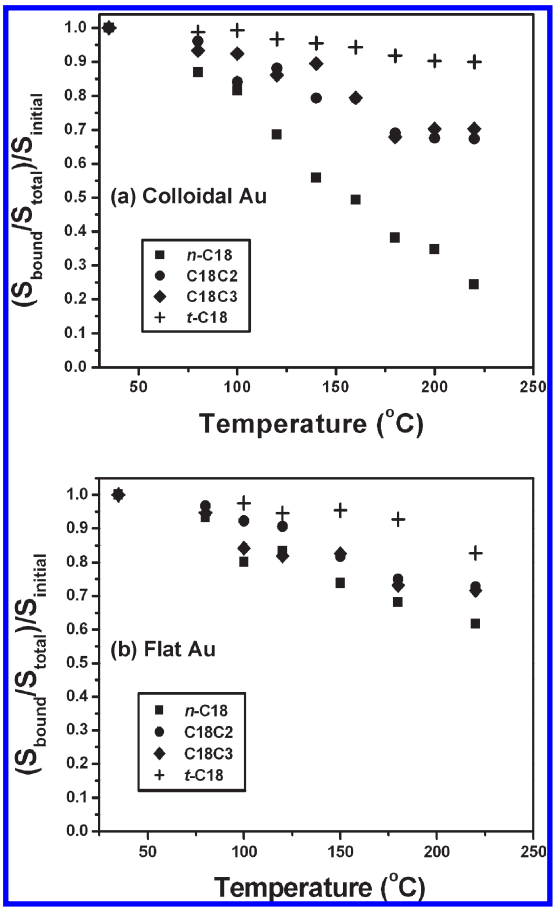

Figure 4. Intensity ratio of sulfur peaks for SAMs on (a) colloidal gold and (b) flat gold as determined by XPS as a function of temperature.

corresponding to unbound thiol or disulfide species appears at 163.5−164 eV.[49,50] As such, we determined S_{bound} by summing the S $2p_{3/2}$ and S $2p_{1/2}$ peak areas corresponding to bound thiol. Furthermore, we determined S_{total} and $S_{initial}$ by summing the peak areas for both bound thiol (S_{bound}) and unbound thiol/disulfide. The results have been interpreted, as described below, on the basis of two general trends in the data.

Figure 4a and 4b show the $(S_{bound}/S_{total})/S_{initial}$ ratio of the SAMs generated on colloidal and flat gold, respectively, as a function of annealing temperature under vacuum. The results indicate that, for both substrates, colloidal and flat gold, the $(S_{bound}/S_{total})/S_{initial}$ ratio for ***n*-C18** decreased faster than those for **C18C2**, **C18C3**, and ***t*-C18**, while the $(S_{bound}/S_{total})/S_{initial}$ ratio for ***t*-C18** decreased the slowest of all. The observed decrease in the $(S_{bound}/S_{total})/S_{initial}$ ratios were similar for **C18C2** and **C18C3** on both substrates, which suggests a comparable thermal stability for both of these SAMs. Based on these data as a whole, we conclude that the relative trend in thermal stabilities of the SAMs under vacuum conditions is ***t*-C18 > C18C2 ≈ C18C3 > *n*-C18**. This trend is consistent with our preliminary examination of the solution-phase thermal stability of these SAMs on flat gold as measured by ellipsometry,[20] our evaluation of the solution-phase thermal stability of these SAMs on large gold nanoparticles (20−50 nm in diameter),[33] and our investigation of the reductive desorption of the SAMs as a function of electric potential.[51]

We note further that the SAMs generated from ***n*-C18** on colloidal gold appear to desorb more readily than those generated from ***n*-C18** on flat gold. Upon heating to 220 °C, for example, ∼60% of the SAM remained on flat gold, whereas ∼30% of the SAM remained on colloidal gold. Interestingly, the thermal stabilities of SAMs generated from **C18C2**, **C18C3**, and ***t*-C18** were largely insensitive to the nature of the gold substrate. Upon heating to 220 °C, for example, ∼75% of the SAM generated from **C18C2** remained on flat gold, whereas ∼70% of this SAM remained on colloidal gold. While it is tempting to attribute the differing behavior to differences in curvature of the gold substrates, other factors might also be involved, including the coalescence of the gold colloidal particles modified with the monodentate ***n*-C18** ligand. Shimizu and co-workers studied the size evolution of alkanethiol-protected colloidal gold upon thermolysis in the solid state and found that the mean diameter of the particles increased upon heating at 150−250 °C.[52] Based on the determination that the melting point of colloidal gold (287 °C) is markedly lower than that of bulk gold (1064 °C), the authors proposed that particle growth was induced by melting of the surfaces of the gold particles, leading to particle growth/coalescence.[52] The coalescence process probably proceeds via (1) desorption of the alkanethiol ligand from the surface of the particle, (2) gold core agglomeration accompanied by the rearrangement of gold atoms, and (3) reprotection by alkanethiol.[39,40,52] It is possible that this dynamic behavior of colloidal gold can be used to rationalize our observation that the SAMs generated from ***n*-C18** on colloidal gold desorb more readily than those generated from ***n*-C18** on flat gold (vide supra). In any event, it appears that the inhibited desorption of the bidentate ligands, **C18C2** and **C18C3**, and particularly the tridentate ligand, ***t*-C18**, leads to an inhibition of the nanoparticle coalescence process. This inhibition undoubtedly arises from the chelate effect, where the degree of chelation is known to correlate with thermal stability.[28,29,33] Consequently, it is plausible that we observed the following trend in thermal stability for MPCs examined in this investigation: ***t*-C18 > C18C2 ≈ C18C3 > *n*-C18**.

Conclusions

We examined the thermal stability of SAMs derived from ***n*-C18**, **C18C2**, **C18C3**, and ***t*-C18** on both colloidal and flat gold. We used UV−visible spectrometry to monitor the solution-phase thermal stability of the SAMs on colloidal gold (i.e., MPCs) in solution, finding that the UV spectra of all of the MPCs undergo a red shift upon thermolysis at 120 °C. The observed red shifts ranged from 35 to 70 nm and were interpreted to reflect the three-step process of (1) desorption of the ligand from the surface of the particle, (2) gold core agglomeration, and (3) reprotection by the ligand. Notably, the MPCs coated with monodentate ***n*-C18** exhibit the fastest red shift of the plasmon resonance, but the relative trend for the MPCs coated with multidentate **C18C2**, **C18C3**, and ***t*-C18** could not be readily distinguished. Displacement studies, however, provided additional partial clarification, suggesting the following trend in thermal stability of the MPCs: ***t*-C18 > C18C2 ≈ C18C3 > *n*-C18**. Additional studies by XPS of the solid-state thermolysis of the MPCs and corresponding

(49) Castner, D. G.; Hinds, K.; Grainger, D. W. *Langmuir* **1996**, *12*, 5083.
(50) Bensebaa, B.; Zhou, Y.; Deslandes, Y.; Kruus, E.; Ellis, T. H. *Surf. Sci.* **1998**, *405*, L472.
(51) Wang, W.; Zhang, S.; Chinwangso, P.; Advincula, R. C.; Lee, T. R. *J. Phys. Chem. C* **2009**, *113*, 3717.
(52) Shimizu, T.; Teranishi, T.; Hasegawa, S.; Miyake, M. *J. Phys. Chem. B* **2003**, *107*, 2719.

samples of SAM-coated flat gold gave the same trend. Given that the observed trend in thermal stability correlates directly with the degree of chelation (i.e., tridentate > bidentate > monodentate), we conclude that the chelate effect is primarily responsible for the differing thermal stabilities observed in this investigation.

Acknowledgment. We thank the National Science Foundation (ECCS-0926027), the Texas Center for Superconductivity, and the Robert A. Welch Foundation (Grant E-1320) for generous financial support. We also thank the Royal Thai Government for supporting the predoctoral studies of Ms. Srisombat.